

## Coherent phonon spectroscopy characterization of electronic bands at buried semiconductor heterointerfaces

Kunie Ishioka, Kristina Brixius, Andreas Beyer, Avinash Rustagi, Christopher J. Stanton, Wolfgang Stolz, Kerstin Volz, Ulrich Höfer, and Hrvoje Petek

Citation: *Applied Physics Letters* **108**, 051607 (2016); doi: 10.1063/1.4941397

View online: <http://dx.doi.org/10.1063/1.4941397>

View Table of Contents: <http://scitation.aip.org/content/aip/journal/apl/108/5?ver=pdfcov>

Published by the [AIP Publishing](#)

---

### Articles you may be interested in

Misfit dislocation formation at heterointerfaces in (Al,In)GaN heteroepitaxial layers grown on semipolar free-standing GaN substrates

*J. Appl. Phys.* **109**, 033505 (2011); 10.1063/1.3531577

Structural and vibrational properties of molecular beam epitaxy grown cubic (Al, Ga)N/GaN heterostructures

*J. Appl. Phys.* **89**, 2631 (2001); 10.1063/1.1345858

Resonant Raman scattering from buried Al<sub>x</sub>Ga<sub>1-x</sub>N (x0.17) layers in (Al,Ga,In)N heterostructures

*J. Appl. Phys.* **87**, 2853 (2000); 10.1063/1.372268

Growth, optical, and electron transport studies across isotype n-GaAs/n-Ge heterojunctions

*J. Vac. Sci. Technol. B* **17**, 1003 (1999); 10.1116/1.590684

Evidence for misfit dislocation-related carrier accumulation at the InAs/GaP heterointerface

*Appl. Phys. Lett.* **72**, 2319 (1998); 10.1063/1.121348

---

A promotional banner for Applied Physics Reviews. It features a blue background with a molecular structure graphic on the left. The text 'NEW Special Topic Sections' is prominently displayed in white. Below this, it says 'NOW ONLINE' in yellow, followed by 'Lithium Niobate Properties and Applications: Reviews of Emerging Trends' in white. The AIP Applied Physics Reviews logo is in the bottom right corner.

**NEW Special Topic Sections**

**NOW ONLINE**  
Lithium Niobate Properties and Applications:  
Reviews of Emerging Trends

**AIP** Applied Physics Reviews

## Coherent phonon spectroscopy characterization of electronic bands at buried semiconductor heterointerfaces

Kunie Ishioka,<sup>1,a)</sup> Kristina Brixius,<sup>2</sup> Andreas Beyer,<sup>2</sup> Avinash Rustagi,<sup>3</sup> Christopher J. Stanton,<sup>3</sup> Wolfgang Stolz,<sup>2</sup> Kerstin Volz,<sup>2</sup> Ulrich Höfer,<sup>2</sup> and Hrvoje Petek<sup>4</sup>

<sup>1</sup>*Nano Characterization Unit, National Institute for Materials Science, Tsukuba 305-0047, Japan*

<sup>2</sup>*Faculty of Physics and Materials Sciences Center, Philipps-Universität Marburg, 35032 Marburg, Germany*

<sup>3</sup>*Department of Physics, University of Florida, Gainesville, Florida 32611, USA*

<sup>4</sup>*Department of Physics and Astronomy and Pittsburgh Quantum Institute, University of Pittsburgh, Pittsburgh, Pennsylvania 15260, USA*

(Received 25 November 2015; accepted 22 January 2016; published online 4 February 2016)

We demonstrate an all-optical approach to probe electronic band structure at buried interfaces involving polar semiconductors. Femtosecond optical pulses excite coherent phonons in epitaxial GaP films grown on Si(001) substrate. We find that the coherent phonon amplitude critically depends on the film growth conditions, specifically in the presence of antiphase domains, which are independently characterized by transmission electron microscopy. We determine the Fermi levels at the buried interface of GaP/Si from the coherent phonon amplitudes and demonstrate that the internal electric fields are created in the nominally undoped GaP films as well as the Si substrates, possibly due to the carrier trapping at the antiphase boundaries and/or at the interface. © 2016 AIP Publishing LLC. [<http://dx.doi.org/10.1063/1.4941397>]

Characterization of the electronic energy states at buried hetero-interfaces is one of the most pressing issues in device physics. Simple estimations based on the electron affinities of the two semiconductors<sup>1</sup> often fail due to the formation of new interfacial chemical bonds, extended defects, crystalline morphologies, and intermixing.<sup>2–4</sup> It is therefore crucial to determine the band alignment by measuring actual interfaces. Photoemission spectroscopy, which is the standard technique to directly evaluate the electronic states at surfaces and interfaces with thin overlayers,<sup>5</sup> cannot be applied to deeply buried interfaces due to the limited probing depth ( $\leq 5$  nm). Capacitance-voltage measurements<sup>6</sup> and internal photoemission spectroscopy<sup>7</sup> can be applied to thicker overlayers, but they can be influenced by the carrier transport in the overlayers. Complementary all-optical techniques are desirable to evaluate the electronic states of deeply buried interfaces.

In polar semiconductors, the collective oscillations of charge carriers (plasmas) couple with the longitudinal optical (LO) phonons via the Coulomb interaction.<sup>8</sup> The frequency of the resulting LO phonon-plasmon coupled (LOPC) mode depends crucially on carrier density and plasma damping rate. Raman observation of the LOPC mode has been employed extensively to determine the carrier distributions within polar semiconductors and at their interfaces.<sup>9–11</sup> The LOPC mode can also be excited as a coherent oscillation by femtosecond optical pulses.<sup>12,13</sup> Because coherent LOPC mode is generated predominantly by the instantaneous screening of the surface field by photoexcited electrons and holes,<sup>14,15</sup> the amplitude of the oscillation can be a quantitative measure for the pre-existing electric field and the resulting electronic band structure. Thus, coherent phonon spectroscopy is promising as an all-optical evaluation technique of the electronic states at buried interfaces including polar semiconductors.

The growth of group III-V semiconductors on Si is motivated by the potential for incorporating optoelectronic functions into Si based devices. GaP, an important material for light emitting diodes, photovoltaics, and photocatalysts, is particularly interesting because it has a good epitaxial relationship with the Si(001) surface.<sup>16–19</sup> In this letter, we report on the experimental characterization of the Fermi level at GaP/Si(001) interfaces by coherent phonon spectroscopy. The formation of a hetero-interface may affect the electronic structure of GaP significantly through, e.g., unintentional doping and differently charged pinning centers, even though the GaP films are not intentionally doped. We find that the Fermi level correlates with the density of antiphase domains (APDs) in GaP films and predicts the electronic band profiles by theoretical simulations.

The samples studied are nominally undoped GaP layers grown by metal organic vapour phase epitaxy on the *n*-type Si(001) substrates under three different conditions.<sup>20</sup> The GaP film samples I and II are grown at 675 and 450 °C on the Si(001) substrate with a very small miscut angle, whereas sample III is grown at 575 °C on a Si(001) substrate with a larger miscut angle. Whereas all the films are free from extended planar defects, the different growth conditions introduce different densities and shapes of APDs, in which the direction of the Ga-P bonds are reversed with respect to the main phase [Figs. 1(a) and 1(b)]. Sample I has self-annihilated (kinked) APDs with boundaries on the {112} and {110} planes [Fig. 1(c)], whereas sample II has APD boundaries vertically penetrating the film on the {110} planes [Fig. 1(d)]. Sample III, by contrast, has only a few small ( $< 5$  nm in height) APDs [Fig. 1(e)]. The film thicknesses for samples I, II, and III measured by x-ray diffraction are 57, 55, and 45 nm. We note that the unintentional doping levels of the GaP thin films cannot be determined directly, e.g., by Hall measurements, because they are grown on conductive substrates. Pump-probe reflectivity measurements are performed

<sup>a)</sup>ishioka.kunie@nims.go.jp

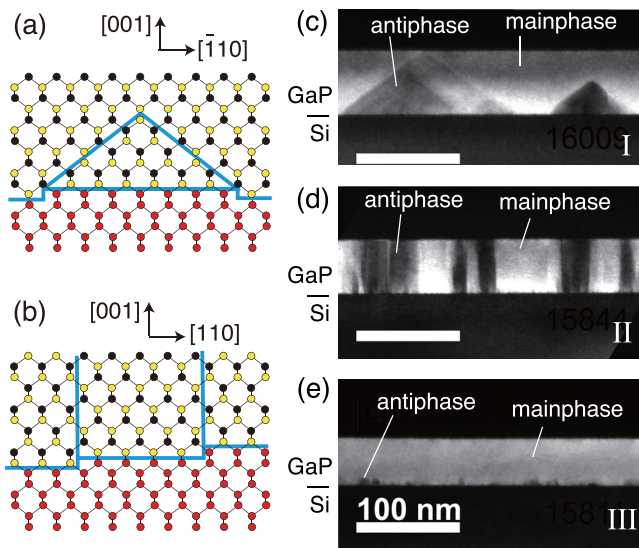


FIG. 1. (a) and (b) Atomic models for antiphase domains (APDs) of GaP on Si(001) with boundaries on the  $\{112\}$  (a) and  $\{110\}$  planes (b). Yellow, black, and red circles represent Ga, P, and Si atoms. Blue lines represent APD boundaries. (c)–(e) Cross-sectional (002) dark field images of GaP layers grown on Si(001) for samples I, II, and III. The APDs exhibit dark contrast with respect to the bright main phase. The viewing direction is  $[110]$  for all the images.

at room temperature in a near back-reflection configuration using optical pulses of  $\sim 10$  fs duration and 400-nm wavelength (3.1-eV photon energy).<sup>20</sup> The effective probing depth  $[(2\alpha)^{-1} = 58$  nm for GaP with  $\alpha$  as the absorption coefficient<sup>21</sup>] is comparable to the GaP layer thicknesses. The pump-induced change in the anisotropic reflectivity  $\Delta R_{eo}$  is measured as a function of time delay between the pump and probe pulses.

Figure 2 compares the oscillatory parts of  $\Delta R_{eo}/R$  and their Fourier-transformed (FT) spectra for the GaP/Si samples. The coherent responses of samples I and II roughly resemble those of the  $p$ -type GaP(001), which we studied previously<sup>13</sup> and are also shown in Fig. 2. They are all dominated by a long-lived LO phonon at 12 THz, whose amplitude is nearly independent of pump density, and a faster-decaying LOPC mode with the amplitude growing with the pump density.<sup>20</sup> GaP/Si samples I and II also feature relatively weak oscillations at 11 and 15.6 THz, both of which are absent from the bulk GaP. The frequencies agree with those of the TO phonon of GaP and the optical phonon of Si, respectively. For sample III, by contrast, the LOPC and LO modes from the GaP overlayer have much smaller amplitudes than the optical phonon of the Si substrate, even though its thickness is comparable to the other samples.

The amplitudes, frequencies, and dephasing rates of the coherent phonon modes are obtained from fitting the time-domain data to damped harmonic functions.<sup>20</sup> The photocarrier density-dependent frequency and dephasing rate of the LOPC mode, shown in Fig. 3, confirm that this mode involves the photoexcited plasma. Static dielectric model<sup>20</sup> roughly reproduces the frequency and dephasing rate assuming heavy damping ( $\gamma = 25$ –30 THz) of the plasma. Based on the previous study,<sup>13</sup> we attribute the LOPC mode to the mixed electron-hole plasma. Unlike when GaAs is photoexcited at 800 nm,<sup>22</sup> the electrons photoexcited in GaP at

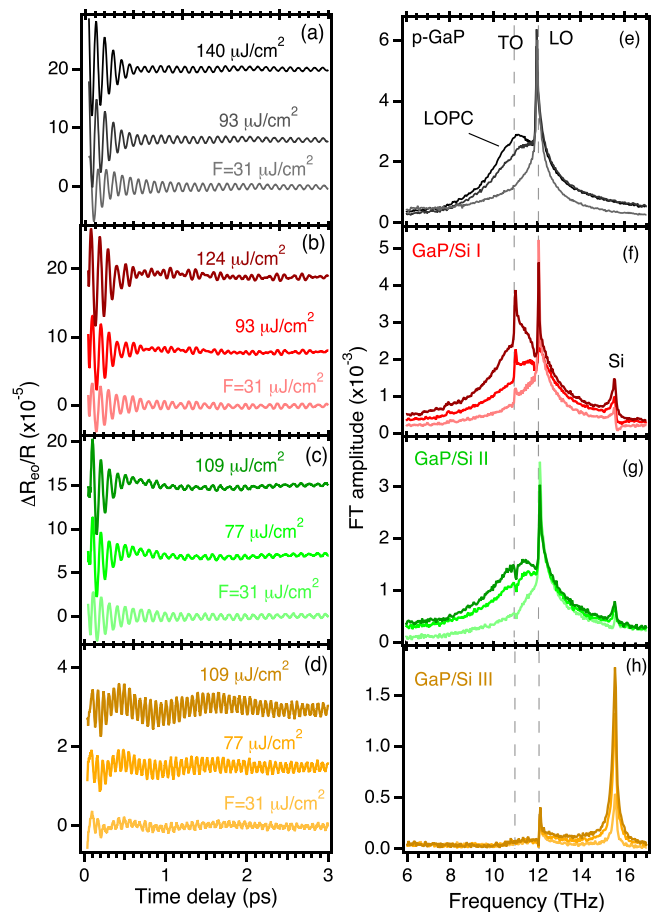


FIG. 2. Oscillatory part of the anisotropic reflectivity changes (a)–(d) and their FT spectra (e)–(h) for bulk  $p$ -doped GaP (a) and (e), GaP/Si samples I (b) and (f), II (c) and (g), and III (d) and (h) at different pump energy densities  $F$ . Traces in (a)–(d) are offset for clarity. LO and TO frequencies are indicated by broken lines in (e)–(h).

400 nm are scattered almost instantaneously into the X and L satellite valleys that have nearly as large effective masses and damping rates as the heavy holes. The mixed plasma consisting of electrons and holes therefore give rise to an effectively single-component, heavily-damped LOPC mode, like when GaAs is excited with 400 nm light.<sup>23</sup>

The amplitude of the LOPC mode varies by almost an order of magnitude among the GaP/Si samples, as shown

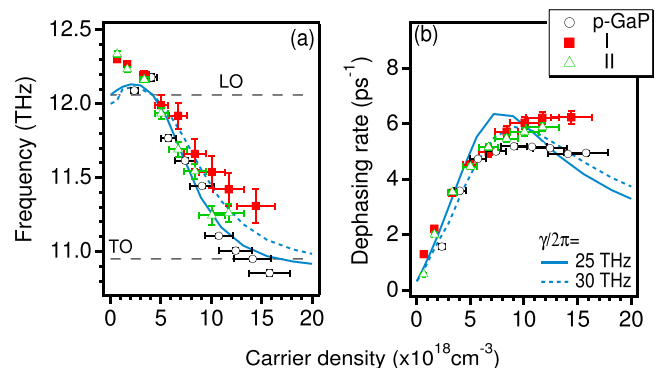


FIG. 3. (a) Frequency and (b) dephasing rate of the LOPC mode of GaP/Si samples and  $p$ -doped GaP as a function of photoexcited carrier density. The solid and dotted curves in (a) and (b) represent the LOPC frequency and dephasing rate calculated using the static dielectric model in the case of the plasma damping rate  $\gamma/2\pi = 25$  and 30 THz, respectively.<sup>20</sup> The LO and TO phonon frequencies are indicated by broken lines in (a).

with broken lines in Fig. 4. The excitation of the coherent LOPC mode of GaP is dominated by the transient depletion field screening (TDFS) mechanism,<sup>13</sup> in which the ultrafast drift of photoexcited electrons and holes, shown in insets of Fig. 4, suddenly screen the pre-existing surface electric field in the depletion region.<sup>14,15</sup> The variation in the LOPC amplitude among GaP/Si samples can therefore be a measure of the variation of the internal electric field within the GaP layers; large (small) LOPC amplitude implies steep (flat) band bending before photoexcitation.

To estimate the band bending quantitatively, we need to establish the relation between the LOPC amplitude and the electric field. This can be done by comparing the LOPC modes of differently doped bulk GaP crystals, which were measured under the same experimental conditions.<sup>13</sup> The symbols in Fig. 4 plot the LOPC amplitudes of (001)-oriented GaP as a function of the Fermi level  $E_F$ . Because the bands bend up (down) toward the surface for the  $p$ -type ( $n$ -type) surface, as illustrated by insets in Fig. 4, we fit the amplitudes with a linear function  $\Delta R_{\text{LOPC}}/R = C|E_F - E_{\text{pin}}|$  with  $C$  and  $E_{\text{pin}}$  as parameters.<sup>20</sup> We obtain the pinning energy at the GaP/air surface  $E_{\text{pin}} \simeq E_v^s + 1.8 \text{ eV}$ , with  $E_v^s$  being the valence band maximum at the surface. This value is close to that reported for the GaP(110)/vacuum surface,  $E_v^s + 1.6 \text{ eV}$ .<sup>24</sup>

We now estimate the Fermi levels for the GaP/Si(001) samples assuming that they are pinned at the surface by the same electronic states as for the bulk GaP(001). This is a reasonable assumption because our GaP films have nearly atomically flat surfaces. From crossings between the amplitudes (broken lines in Fig. 4) and the linear fit (solid line), we obtain  $E_F$  within the films of 0.1, 0.6, and 1.7–1.9 eV above  $E_v$  for samples I, II, and III.

We consider two possible explanations for different interface Fermi levels of the differently grown GaP films.

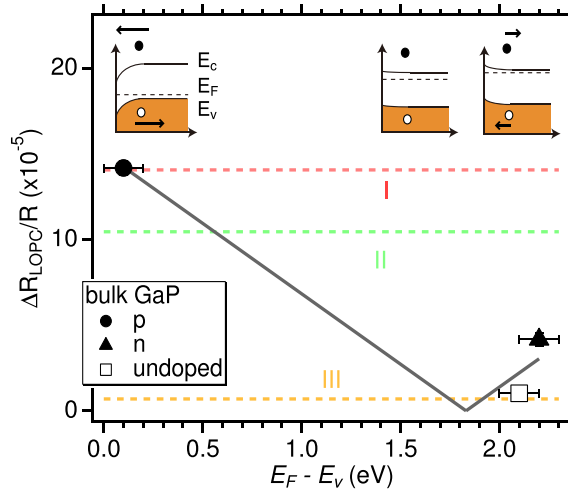


FIG. 4. LOPC amplitude for bulk GaP(001) crystals (symbols) as a function of Fermi level  $E_F$  with respect to the valence band maximum  $E_v$  deep in the bulk. Insets schematically illustrate the bands in the surface depletion region for different dopings, with arrows indicating initial drifts of photoexcited carriers involved in the TDFS mechanism. Solid lines represent the fitting of the symbols to a linear function  $\Delta R_{\text{LOPC}}/R = C|E_F - E_{\text{pin}}|$ . Horizontal broken lines denote the LOPC amplitudes for the GaP/Si(001) samples, whose crossings with the solid line give the values for  $E_F$  deep in the film. The pump energy density is  $F = 109 \mu\text{J}/\text{cm}^2$  for all the GaP(001) and GaP/Si(001) samples.

One is that the GaP films are unintentionally doped at different densities. The estimated  $E_F$  shows no correlation with the film growth temperature and thus excludes the possibility of doping via intermixing of Si atoms. However, we find a correlation between  $E_F$  and the APD density, which would suggest higher doping for higher APD density. Though the conventional atomic models of APD boundaries [Figs. 1(a) and 1(b)] are neutral with equal numbers of Ga-Ga and P-P bonds, the actual boundaries can deviate from the stoichiometric models at the atomic scale, as reported in a previous TEM study,<sup>25</sup> and thereby introduce charges localized at the APD boundaries throughout the GaP layer thickness. Another possible explanation is that the GaP films are nearly intrinsic but the interface Fermi level is determined by trapping centers at the GaP/Si interface, whose energy levels and charge states depend on the film growth conditions. It is plausible that both of the two scenarios contribute to determining the interface Fermi level.

Because the actual charge distributions within the GaP films and the energy levels of the interfacial pinning centers are unknown, we model the electronic energy bands by making several simplifying assumptions.<sup>20</sup> We solve the Poisson equation for electric potential assuming the charge neutrality between the GaP layer and the depletion region of  $n$ -type Si. We consider two limiting cases in the charge distribution; in one case, the electric charges distribute uniformly over the GaP film. This would model the GaP film unintentionally doped by the carrier trapping at the APD boundaries that extends over the whole thickness of the film. In another case, charges are mostly trapped at the interface and the surface. This would model the nearly intrinsic GaP film whose  $E_F$  is pinned by the trap centers at the interface and the surface. The actual situation probably lies between the two limiting cases. Figure 5 compares the energy bands calculated in these two limiting cases. The results are qualitatively similar, except that the bands are curved for uniform charge distribution and straight for the Fermi level pinning at the interface. In both cases, the band bending within the GaP film is accompanied by a bending of similar magnitude in the Si substrate. Though our model is very simple, our calculations give a qualitative picture of the band profiles within the GaP film without detailed knowledge of the charge distribution in the GaP films and the trap states at the interface.

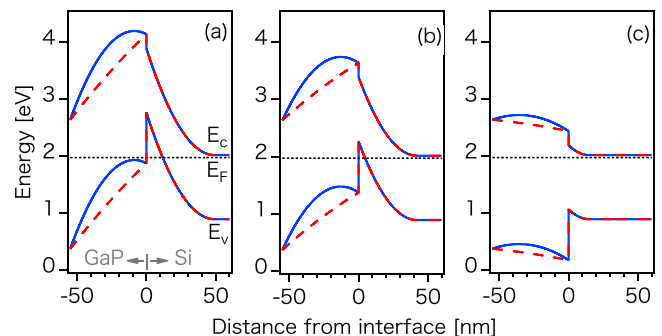


FIG. 5. Energy bands calculated to reproduce the experimental values of  $E_F$  for GaP/Si samples I (a), II (b), and III (c).  $E_F$ ,  $E_c$ , and  $E_v$  denote Fermi level, conduction band minimum and valence band maximum. Solid and broken curves are, respectively, calculated uniform charge distribution over the GaP film and Fermi level pinning at the interface.<sup>20</sup>

The present method has an advantage that we can estimate the electronic band profiles also in non-polar Si. The band bending in Si cannot be obtained directly from the Si phonon amplitude, because the TDFS mechanism works only on the polar, infrared active phonon modes, which the Si phonon is not. Coherent Si phonons are generated solely via the impulsive stimulated Raman scattering mechanism through deformation potential interaction,<sup>20,26</sup> which is independent of the magnitude of the surface band bending.

In conclusion, the lattice-matched GaP/Si(001) interfaces give rise to the coherent LOPC mode, whose amplitude can be used as a measure for the internal electric fields within the GaP films. We find that higher density of APDs in the GaP film leads to larger electric field as probed by the amplitude of the coherent phonons. Our approach is also useful for heterostructures involving other polar semiconductors, such as GaAs and InN, whose coherent phonons can be excited via TDFS mechanism. We thus demonstrate the applicability of the coherent phonon spectroscopy to the nondestructive characterization of the electronic states at buried interfaces.

This work was partly supported by the Deutsche Forschungsgemeinschaft through SFB 1083 and HO2295/8, as well as by NSF Grant DMR-1311845 (Petek) and DMR-1311849 (Stanton). H.P. thanks support from the Alexander von Humboldt Foundation and the Chinese Academy of Sciences President's International Fellowship Initiative.

<sup>1</sup>H. Kroemer, *Surf. Sci.* **132**, 543 (1983).

<sup>2</sup>R. Bauer and H. Sang, *Surf. Sci.* **132**, 479 (1983).

<sup>3</sup>J. Woodall, G. Pettit, T. Jackson, C. Lanza, K. Kavanagh, and J. Mayer, *Phys. Rev. Lett.* **51**, 1783 (1983).

- <sup>4</sup>J. Silberman, T. Delyon, and J. Woodall, *Appl. Phys. Lett.* **59**, 3300 (1991).
- <sup>5</sup>P. Sippel, O. Supplie, M. May, R. Eichberger, and T. Hannappel, *Phys. Rev. B* **89**, 165312 (2014).
- <sup>6</sup>T. Katoda and M. Kishi, *J. Electron. Mater.* **9**, 783 (1980).
- <sup>7</sup>I. Sakata and H. Kawanami, *Appl. Phys. Express* **1**, 091201 (2008).
- <sup>8</sup>B. B. Varga, *Phys. Rev.* **137**, A1896 (1965).
- <sup>9</sup>G. Irmer, J. Monecke, and W. Siegel, *Cryst. Res. Technol.* **20**, 1125 (1985).
- <sup>10</sup>G. Irmer and W. Siegel, *Phys. Status Solidi A* **105**, 549 (1988).
- <sup>11</sup>S. Nakashima, H. Yugami, A. Fujii, M. Hangyo, and H. Yamanaka, *J. Appl. Phys.* **64**, 3067 (1988).
- <sup>12</sup>Y.-M. Chang, *Appl. Phys. Lett.* **82**, 1781 (2003).
- <sup>13</sup>K. Ishioka, K. Brixius, U. Höfer, A. Rustagi, E. Thatcher, C. Stanton, and H. Petek, *Phys. Rev. B* **92**, 205203 (2015).
- <sup>14</sup>T. Dekorsy, T. Pfeifer, W. Kütt, and H. Kurz, *Phys. Rev. B* **47**, 3842 (1993).
- <sup>15</sup>A. V. Kuznetsov and C. J. Stanton, *Phys. Rev. B* **51**, 7555 (1995).
- <sup>16</sup>T. Thanh, C. Robert, W. Guo, A. Letoublon, C. Cornet, G. Elias, A. Ponchet, T. Rohel, N. Bertru, A. Balocchi, O. Durand, J. Micha, M. Perrin, S. Loualiche, X. Marie, and A. Corre, *J. Appl. Phys.* **112**, 053521 (2012).
- <sup>17</sup>A. Lin, M. Fejer, and J. Harris, *J. Cryst. Growth* **363**, 258 (2013).
- <sup>18</sup>O. Supplie, M. May, G. Steinbach, O. Romanyuk, F. Grosse, A. Nägelein, P. Kleinschmidt, S. Brückner, and T. Hannappel, *J. Phys. Chem. Lett.* **6**, 464 (2015).
- <sup>19</sup>K. Volz, A. Beyer, W. Witte, J. Ohlmann, I. Nemeth, B. Kunert, and W. Stolz, *J. Cryst. Growth* **315**, 37 (2011).
- <sup>20</sup>See supplementary material at <http://dx.doi.org/10.1063/1.4941397> for the details of the sample preparation, pump-probe measurements, and data analyses.
- <sup>21</sup>D. Aspnes and A. Studna, *Phys. Rev. B* **27**, 985 (1983).
- <sup>22</sup>Y.-M. Chang, *Appl. Phys. Lett.* **80**, 2487 (2002).
- <sup>23</sup>A. Basak, H. Petek, K. Ishioka, E. Thatcher, and C. Stanton, *Phys. Rev. B* **91**, 125201 (2015).
- <sup>24</sup>P. Chiaradia, M. Fanfoni, P. Nataletti, P. D. Padova, L. Brillson, M. Slade, R. Viturro, D. Kilday, and G. Margaritondo, *Phys. Rev. B* **39**, 5128 (1989).
- <sup>25</sup>A. Beyer, B. Haas, K. Gries, K. Werner, M. Luysberg, W. Stolz, and K. Volz, *Appl. Phys. Lett.* **103**, 032107 (2013).
- <sup>26</sup>M. Hase, M. Kitajima, A. Constantinescu, and H. Petek, *Nature* **426**, 51 (2003).

# Coherent phonon spectroscopy characterization of electronic bands at buried semiconductor heterointerfaces: Supplementary Material

Kunie Ishioka,<sup>1</sup> Kristina Brixius,<sup>2</sup> Andreas Beyer,<sup>2</sup> Avinash Rustagi,<sup>3</sup> Christopher J. Stanton,<sup>3</sup> Wolfgang Stolz,<sup>2</sup> Kerstin Volz,<sup>2</sup> Ulrich Höfer,<sup>2</sup> and Hrvoje Petek<sup>4</sup>

<sup>1</sup>*Nano Characterization Unit, National Institute for Materials Science, Tsukuba, 305-0047 Japan*

<sup>2</sup>*Faculty of Physics and Materials Sciences Center,  
Philipps-Universität Marburg, 35032 Marburg, Germany*

<sup>3</sup>*Department of Physics, University of Florida, Gainesville, FL 32611 USA*

<sup>4</sup>*Department of Physics and Astronomy and Pittsburgh Quantum Institute,  
University of Pittsburgh, Pittsburgh, PA 15260, USA*

(Dated: September 6, 2016)

## I. SAMPLE PREPARATION

Nominally undoped GaP layers are grown by metal organic vapour phase epitaxy on the  $n$ -type Si(001) substrates under three different conditions. For the GaP/Si sample I, the “exact” Si (001) substrate with a  $0.1^\circ$  miscut in the [110] direction is used. First, a homoepitaxial Si-buffer layer is deposited on the Si substrate and annealed in  $H_2$  atmosphere to form double steps. The GaP nucleation layer of 7 nm in thickness is then grown at  $450^\circ\text{C}$ , followed by the growth at  $675^\circ\text{C}$ . This procedure minimizes the density of planar defects and enhances the self-annihilation (kinking) of antiphase domains (APDs) with boundaries on the  $\{112\}$  and  $\{110\}$  planes [Fig. 1c]. Sample II is grown in the same procedures as sample I, except that the second step of the GaP film growth is carried out at  $450^\circ\text{C}$ . This leads to the APDs penetrating the film along the vertical  $\{110\}$  planes [Fig. 1d]. For sample III, a Si(001) substrate with a larger miscut angle of  $2^\circ$  is used to effectively suppress the formation of the monoatomic steps of the substrate and thereby APDs [Fig. 1e]. Following the same nucleation procedure as samples I and II, the GaP film is grown at  $575^\circ\text{C}$ . The film thicknesses for samples I, II and III are measured by x-ray diffraction to be 57, 55 and 45 nm. More details of the sample preparation and transmission electron microscopic evaluation of APDs are described elsewhere [1–3].

Whereas Si atoms in GaP can act as shallow donors when substituting the Ga site [4], we believe that unintentional doping of the GaP films by Si atoms due to the cross diffusion is very limited because of our relatively low growth temperature. Indeed, the Fermi level obtained from the coherent phonon spectroscopy [broken lines in Fig. 4] exhibits no clear correlation with the film growth temperature. We note that the unintentional doping levels of the GaP films cannot be determined directly by Hall measurements, because they are grown on the conductive ( $n$ -doped) Si substrate.

We also use (001)-oriented GaP wafers purchased from the MTI Corp as the standard samples to obtain the relationship between the coherent phonon amplitude and the Fermi level [symbols in Fig. 5]. The  $n$ - and  $p$ -doped GaP samples are doped with S and Zn impurities at  $5\pm 3 \times 10^{17}$  and  $6.95 \times 10^{17} \text{ cm}^{-3}$  carrier densities, respectively. The undoped sample has  $n$ -type conduction with carrier concentration of  $5\pm 1 \times 10^{16} \text{ cm}^{-3}$ .

## II. PUMP-PROBE EXPERIMENTS

Degenerate pump-probe reflectivity measurements are performed in ambient conditions with laser pulses of 400-nm wavelength (3.1-eV photon energy) and 10 fs duration. The 400-nm photons can excite electrons and holes near the  $\Gamma$  point across the direct band gap of GaP of 2.78 eV. The photoexcited electrons and holes are scattered into the lower X and L valleys and into the heavy hole band by the time of the formation of the LO phonon-plasmon coupled (LOPC) mode [5]. The optical penetration depth of the 400-nm light is given by  $\alpha^{-1}=116 \text{ nm}$  [6] with  $\alpha$  the absorption coefficient. The probing depth of the 400-nm light is  $(2\alpha)^{-1}=58 \text{ nm}$ , since the reflected probe light passes the medium twice.

The pump-induced change in the anisotropic reflectivity ( $\Delta R_{eo} = \Delta R_H - \Delta R_V$ ) is measured in the “electro-optic” (EO) configuration by detecting the difference between the vertically (V) and horizontally (H) polarized components of the reflected probe light. The samples are oriented so that their [011] and  $[0\bar{1}1]$  crystallographic axes point in the V and H directions. Linearly polarized pump and probe beams are incident on the sample in the near back-reflection configuration with angles of  $< 15^\circ$  and  $< 5^\circ$  from the surface normal. In this near back-reflection geometry from the (001) surface, the coherent TO phonon is neither excited nor detected according to the Raman selection rules. The pump and probe laser spots on the sample are  $2d_b=23 \mu\text{m}$  in diameter. The transient reflectivity signal is digitized

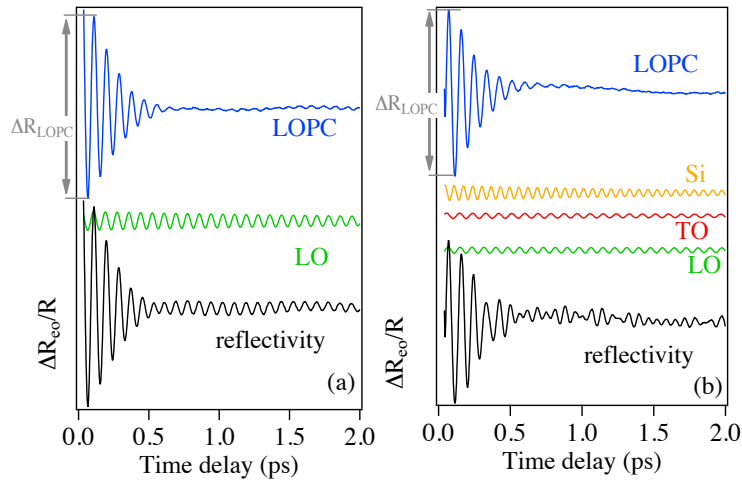


FIG. S1: (Color Online.) Oscillatory parts of the anisotropic reflectivity changes (bottom traces), together with their phonon mode components, for p-doped GaP (a) and GaP/Si sample I (b). The LO, TO and Si oscillations are obtained from fitting the reflectivity oscillation after 1 ps. The LOPC oscillation is obtained by subtracting their sum from the reflectivity oscillations.

and averaged with a 12-bit digital oscilloscope while time delay between pump and probe pulses is scanned repetitively at a 20 Hz rate.

### III. ANALYSES OF EXPERIMENTAL DATA

#### A. Obtaining oscillation parameters from time-domain fittings

Transient reflectivity signals obtained from the pump-probe measurements consist of non-oscillatory electric components and oscillatory phonon components. We first fit the non-oscillatory parts to multiple exponential functions and subtract them from the signals to obtain the oscillatory components. The oscillatory components are then fitted to a linear combination of damped harmonic functions, each of which is expressed by:

$$f_i(t) = \Delta R_i \exp(-\Gamma_i t) \sin[2\pi\nu_i t + \psi_i], \quad (\text{S1})$$

to obtain the amplitudes  $\Delta R_i$ , the dephasing rates  $\Gamma_i$ , and the frequencies  $\nu_i$ , where  $i$  corresponds to either of the LO, LOPC, TO and Si phonon modes. Fitting to a quadruple damped harmonic function is not complicated in the present case, because three (LO, TO, Si) of the four oscillations are long living and clearly separated in the frequency. We therefore start by fitting the reflectivity oscillation after 1 ps, by which the LOPC mode is damped, to a triple damped harmonic function to roughly determine the parameters for the three modes. We then fit the reflectivity oscillation for the whole time (typically 0.1 – 12 ps) to a quadruple damped harmonic function to precisely determine all the oscillation parameters.

The linearly chirped damped harmonic function gives a reasonable approximation for the frequency and dephasing rate of the fast-decaying LOPC mode, which are plotted in Fig. 3. If we perform time-windowed analyses, as we did in our previous study on bulk GaP [5], we find the LOPC frequency to be dependent on time. Moreover, during its first few cycles, the LOPC amplitude often increases and then decreases with time. The situation leads to a very large uncertainty in the determination of the LOPC amplitude by fitting to a damped harmonic function. Because the LOPC amplitude is a key issue in the present study, we obtain the LOPC amplitude as follows: we start by fitting the reflectivity oscillation after 1 ps to the triple damped harmonic function corresponding to the LO, TO and Si modes, as described above. We then extrapolate the triple damped harmonic function to time zero, as shown in Fig. S1, and subtract it from the oscillatory reflectivity signal to obtain the LOPC oscillation. We take the difference between the maximum and minimum of the LOPC oscillation as its amplitude,  $\Delta R_{\text{LOPC}}$ .

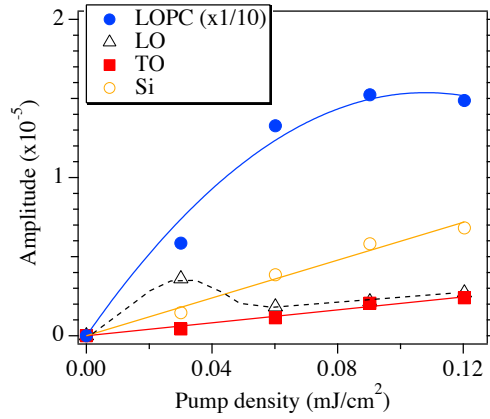


FIG. S2: (Color Online.) Amplitudes of the coherent phonon modes for GaP/Si sample I as a function of pump density.

### B. Pump power and pulse duration dependences

We find the frequencies and dephasing rates of the LOPC mode, summarized in Fig. 3, depend on the pump pulse energy  $F$ . This clearly indicates that the LOPC mode is coupled with photoexcited carriers rather than impurity doped carriers. The frequency and dephasing rate are reproduced reasonably by the real and imaginary parts of  $\omega$  that satisfy:

$$\varepsilon(\omega) = \varepsilon_{\infty} \left[ 1 + \frac{\Omega_{\text{LO}}^2 - \Omega_{\text{TO}}^2}{\Omega_{\text{TO}}^2 - i\Gamma\omega - \omega^2} - \frac{\omega_p^2}{\omega^2 + i\gamma_p\omega} \right] = 0, \quad (\text{S2})$$

with  $\gamma_p = 25 - 30$  THz, as shown in Fig. 3. Here  $\varepsilon_{\infty}$  is the high frequency dielectric constant,  $\Omega_{\text{LO}}$  and  $\Omega_{\text{TO}}$ , the LO and TO phonon frequencies,  $\Gamma$ , the LO phonon dephasing rate,  $\omega_p = \sqrt{4\pi N e^2 / m^* \varepsilon_{\infty}}$ , the plasma frequency,  $N = (1 - R)F\alpha / \pi d_b^2$ , the plasma density,  $m^*$ , the effective mass, and  $\gamma_p$ , the plasma damping rate. The amplitude of the LOPC mode increases with  $F$  until it reaches saturation, while that of the LO mode hardly grows, as shown in Fig. S2. The saturation is attributed to the complete screening of the pre-existing electric field by photoexcited carriers in the transient depletion field screening (TDFS) mechanism, which will be described in the following section.

Though we have not done so in the present study, varying the pulse width can affect the amplitude of a coherent oscillation. Consider an optical pulse given by:

$$E_c(t, \tau_0) = E_0 \exp\left(-\frac{t^2}{\tau_0^2}\right) \exp(i\omega_L t) \quad (\text{S3})$$

with center frequency  $\omega_L$  and duration  $\tau_0$ . The spectral profile of this pulse is given by

$$I(\omega, \tau_0) = \left| \int_{-\infty}^{+\infty} |E_c(t, \tau_0)|^2 e^{i\omega t} dt \right|. \quad (\text{S4})$$

The amplitude of coherent oscillation at  $\Omega$  is proportional to  $I(\omega = \Omega, \tau_0)$ , if other parameters such as pump pulse energy  $F$  is fixed, in the present low pump density regime.

The frequencies and dephasing rates of the LO, TO and Si phonon modes are found to be independent of  $F$  in the present low pump energy regime. The amplitude of the TO and Si phonon modes grow linearly with  $F$ , whereas that of the LO mode saturates at very low pump density, as shown in Fig. S2.

### C. Generation mechanisms of coherent phonons

Coherent LOPC mode of GaP is generated predominantly via the TDFS mechanism, in which photoexcited carriers suddenly screen the pre-existing electric field in the surface depletion layer [7, 8]. Since the driving force for the TDFS mechanism does not depend on the polarization angle  $\theta$  of the pump light for isotropic crystals, the generation mechanism can be experimentally confirmed by measuring the  $\theta$ -dependence of the LOPC amplitude. We find the amplitude is proportional to  $A + B \cos 2\theta$ , with the isotropic component  $A$  arising from TDFS being much larger than

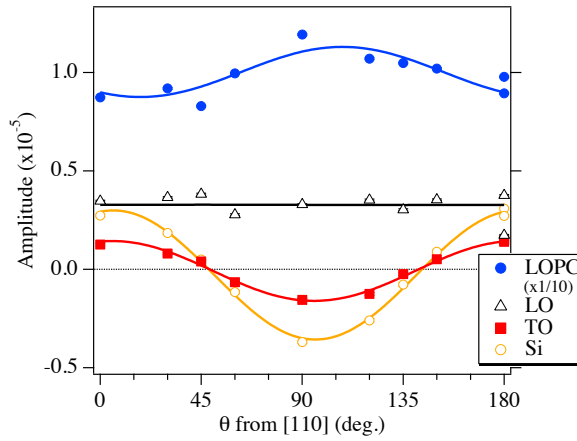


FIG. S3: (Color Online.) Amplitude  $\Delta R_i/R$  of the coherent phonon modes from GaP/Si sample I as a function of pump polarization angle  $\theta$ . The probe polarization is fixed to be parallel to the  $[100]$  axis ( $45^\circ$  from vertical) for the EO detection. Solid curves show the fitting of the amplitudes to  $A + B \cos 2\theta$ .

the anisotropic component  $B$  arising from the impulsive stimulated Raman scattering (ISRS), as reported in Ref. [5] for bulk GaP and shown for GaP/Si sample in Fig. S3.

The TDFS mechanism requires the phonon mode to be polar, *i.e.*, infrared active. In the surface depletion region of polar semiconductors, the equilibrium positions of the cations and anions are shifted with respect to those in the bulk because of the pre-existing electric field. Screening of the pre-existing field by photoexcited carriers suddenly shifts the equilibrium positions of ions closer to the bulk positions, to an extent that depends on the carrier density. The TDFS driving force will not grow with increasing carrier density, once the pre-existing field is completely screened. This leads to the saturation of the LOPC amplitude, as we have seen in Fig. S2.

The TDFS mechanism is not at work for the Si coherent phonon, because Si is a non-polar crystal and its LO phonon is not infrared active. As a result, coherent optical phonons of Si is generated solely via ISRS mechanism through deformation potential [9, 10]. The ISRS force depends on the direction of the electric field through the Raman tensor of the phonon in question. This leads to the  $\cos 2\theta$  dependence for the back-scattering by the LO phonon from the Si(001) surface. This is what is observed for the amplitude of the Si phonon, as shown in Fig. S3.

#### D. Estimation of Fermi levels from LOPC amplitudes

Within the framework of the TDFS mechanism, the driving force, and hence the amplitude, of the coherent LOPC mode is determined by the magnitude of the pre-existing surface electric field, if the high carrier density is sufficiently high to screen the pre-existing field completely. In the present study we aim to estimate the electric field of the GaP/Si samples from the amplitude of the LOPC mode. For this purpose, we first establish the relation between the LOPC amplitude and the Fermi level for differently doped (and well characterized) bulk GaP samples. We note that the pump-probe measurements on the GaP/Si and bulk GaP samples are performed in the same conditions, including the pump pulse energy and duration, and analyzed in the same manner, to make direct comparison of the amplitudes possible.

Symbols in Fig. 4 plot the LOPC amplitudes  $\Delta R_{\text{LOPC}}/R$  for differently doped bulk GaP samples as a function of their Fermi levels  $E_F$ . Pump pulse energy is  $F=109 \mu\text{J}/\text{cm}^2$ , at which the LOPC amplitude is already saturated. We expect that the band bends upward and downward toward the surface for  $n$ - and  $p$ -doped samples, and becomes flat when  $E_F$  matches the pinning level at the GaP/air surface,  $E_{\text{pin}}$ , as shown schematically in the insets of Fig. 4. We therefore fit the symbols to a linear function

$$\frac{\Delta R_{\text{LOPC}}}{R} = C|E_F - E_{\text{pin}}|, \quad (\text{S5})$$

which gives a rough but reasonable interpolation between the symbols. can fit the three symbols for  $C \simeq 8.2 \times 10^{-5}/\text{eV}$  and  $E_{\text{pin}} \simeq E_v + 1.8 \text{ eV}$ , with  $E_v$  being the valence band maximum. The obtained pinning energy  $E_{\text{pin}}$  is close to that reported for the GaP(110)/vacuum surface,  $E_v + 1.6 \text{ eV}$  [11], though there have been no previous report for the GaP(001) surface as far as we are aware of. We note that the value for  $C$  depends on the pump-probe conditions and analyses methods, and cannot be applied directly to LOPC amplitudes obtained from different set of measurements.

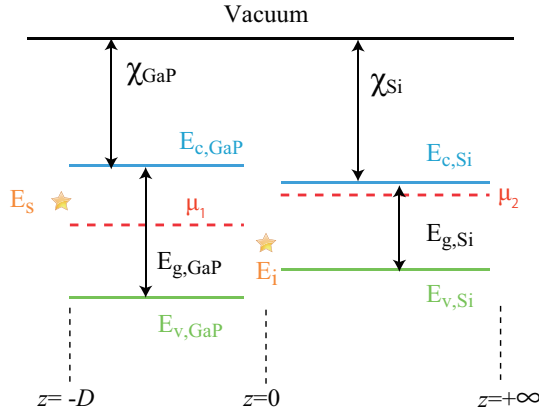


FIG. S4: (Color Online.) Schematic illustrations of bands of GaP and Si before equilibration. Stars denote the energetic positions of the surface and interface states, at which the Fermi level is fixed after the equilibration.

The above fitting function is then used to obtain  $E_F$  of the GaP/Si samples from the LOPC amplitudes measured and analyzed in the same condition.  $\Delta R_{LOPC}/R$  for the three different GaP/Si samples are indicated by the horizontal broken lines in Fig. 4, whose crossings with the fitting function give estimates for their  $E_F$ . The amplitudes for samples I and II have respectively one crossing, at 0.1 and 0.6 eV above  $E_v$ . The crossings occur at lower  $E_F$  than  $E_{pin}$  for both cases, indicating that the bands bend downward toward the surface. For sample III, the amplitude crosses the fitting function twice near  $E_{pin}$ , either of which corresponds to the nearly flat band situation.

#### IV. THEORETICAL CALCULATION OF ENERGY BAND PROFILES

We solve Poisson equation for the electric potential to reconstruct the electronic bands that are consistent with the experimentally obtained  $E_{pin}$  and  $E_F$ . To accurately determine the energy band profile of a GaP/Si interface we would need to know the microscopic details of the interface including the energy, density and distribution of trap states throughout the GaP layer. These details would depend upon the growth conditions of the interface and GaP layer. Because we have little knowledge on such details, however, we aim to acquire a *qualitative* understanding using a simple model with a number of assumptions.

We consider a model one-dimensional heterojunction between GaP and Si to describe a simplified GaP/Si interface. GaP is assumed to be of finite width  $D$  and undoped, whereas Si is infinitely thick and  $n$ -doped with a density of  $N_{Si} = 1 \times 10^{18} \text{ cm}^{-3}$ . The GaP/Si interface is at  $z = 0$  and the GaP/air surface is at  $z = -D$ , as shown in Fig. S4. The conduction band minimum (CBM) and valence band maximum (VBM) of GaP and Si have energy differences of:

$$\begin{aligned} \Delta E_c &\equiv E_{c,GaP} - E_{c,Si} = \chi_{GaP} - \chi_{Si} = 0.25 \text{ eV}, \\ \Delta E_v &\equiv E_{v,Si} - E_{v,GaP} = \chi_{GaP} - \chi_{Si} + E_{g,GaP} - E_{g,Si} = 0.89 \text{ eV}, \end{aligned} \quad (\text{S6})$$

before the alignment of the bands at the surface and interface. In the following we define as  $E_{v,GaP} \equiv 0$  so that  $E_{v,Si} = \Delta E_v$ .

Equilibration between the GaP film and the Si substrate requires a constant Fermi level throughout the heterostructure. We assume that the Fermi level is pinned at the GaP surface by the surface states at  $E_s = 1.6 \text{ eV} + E_{v,GaP}$ , in the same way as bulk GaP, causing the surface band bending and giving rise to the surface electric field. We also assume that the Fermi level at the GaP/Si interface is fixed at  $E_i$ , whose energetic position can depend on the film growth conditions, to model the interface trap states.

The first step to describe the equilibration is to align the Fermi level of Si, with the Fermi level at the interface  $E_i$  at  $z = 0$  and with the chemical potential  $\mu_2$  at large distance  $z$  from the interface. We use the depletion approximation, in which we divide Si substrate into the depletion region in the vicinity of the interface ( $0 < z < W$ ) and the quasi neutral region deeper in the bulk ( $z > W$ ). All the donor atoms in Si are assumed to be ionized, so that the free carrier density of the quasi neutral region is given by the impurity doping density, whereas the charge in the depletion region is dominated by the ionized impurities. Within this approximation, the equilibration of the Fermi levels causes the band bending:

$$V_B = \mu_2 - E_i, \quad (\text{S7})$$

in the depletion region of Si whose width is given by:

$$W = \sqrt{\frac{2\kappa_{\text{Si}}\epsilon_0 V_B}{eN_{\text{Si}}}}. \quad (\text{S8})$$

Thus for Si, the VBM and CBM are approximated by:

$$E_v(z) = \begin{cases} \Delta E_v + V_B \left(1 - \frac{z}{W}\right)^2 & \text{for } 0 < z < W, \\ \Delta E_v & \text{for } z > W, \end{cases} \quad (\text{S9})$$

$$E_c(z) = E_v(z) + E_{g,\text{Si}}.$$

For GaP, which was undoped before the equilibration, we assume that the band offsets at the interface ( $z = 0$ ) do not change on equilibration for the simplicity of the calculations.

$$\begin{aligned} E_c(0^-) &= E_c(0^+) + \Delta E_c, \\ E_v(0^-) &= E_v(0^+) - \Delta E_v. \end{aligned} \quad (\text{S10})$$

This assumption gives a valence band offset of 0.89 eV at the GaP/Si interface, which lies in between those reported in an internal [12] and x-ray [13] photoemission studies as well as in a theoretical modelling [14]. Since the surface pinning level  $E_s$  and the interface Fermi level  $E_i$  are initially different,  $\Delta E_p = E_i - E_s \neq 0$ , the alignment of the pinning energies defines the CBM and VBM at the GaP/air surface:

$$\begin{aligned} E_c(-D) &= E_c(0^-) + \Delta E_p, \\ E_v(-D) &= E_v(0^-) + \Delta E_p. \end{aligned} \quad (\text{S11})$$

The charge that is depleted from the Si interface can get transferred into the GaP layer, with a possibility of being partly trapped at the interface, depending on the film growth conditions. In our simplified model, we parameterize this transfer of charge efficiency by  $\beta$  %. We assume that the transferred charge density is uniformly distributed over the GaP film thickness:

$$N_{\text{GaP}} = \frac{\beta}{100} N_{\text{Si}} \frac{W}{D}. \quad (\text{S12})$$

The transferred charge should be negative, since Si is  $n$ -doped. We can then solve the Poisson equation:

$$\frac{d^2 E_c}{dz^2} = -\frac{e^2 N_{\text{GaP}}}{\kappa_{\text{GaP}} \epsilon_0}, \quad (\text{S13})$$

with the boundary conditions imposed by eqs. (S10) and (S11). Here  $E_c = -e\Phi$  is the spatially varying conduction band minimum, and  $\Phi$  is the electrostatic potential. The bands within the GaP film ( $-D < z < 0$ ) are given by:

$$\begin{aligned} E_c(z) &= E_c(0^-) - \frac{e^2 N_{\text{GaP}} z^2}{2\kappa_{\text{GaP}} \epsilon_0} + \frac{z}{D} \left[ E_c(0^-) - E_c(-D) - \frac{e^2 N_{\text{GaP}} D^2}{2\kappa_{\text{GaP}} \epsilon_0} \right]; \\ E_v(z) &= E_c(z) - E_{g,\text{GaP}}. \end{aligned} \quad (\text{S14})$$

Because we do not know the actual charge distribution, we consider two limiting cases, one with large charge transfer probability ( $\beta = 100\%$ ) and another with small probability ( $\beta = 10\%$ ). In case of  $\beta = 100\%$ , the bands within the GaP film are determined by the uniformly distributed charge density, whereas no charge accumulation at the surface or interface is taken into account [15]. This would model the case that the GaP films have unintentional doping due to *e.g.* the charges localized at the antiphase domain (APD) boundaries, which extends over the entire GaP thickness. Solid curves in Fig. 5 show the bands calculated in the case of  $\beta = 100\%$  for different values of  $E_i$  to reproduce the experimentally obtained  $E_F$  of GaP at the interface. In this case, the bands in the GaP film are curved due to the screening of the charges.

In case of  $\beta = 10\%$ , the GaP film itself remains nearly intrinsic, and the bands within the GaP film are determined by the pinning by the charged centers at the interface as well as at the surface. Broken curves in Fig. 5 show the bands calculated in the case of  $\beta = 10\%$  for different values of  $E_i$ . In this case, the bands are more linear than the case of larger  $\beta$ , because there is little screening within the GaP film. We note that the electric displacement across the interface is not continuous, since we fix the band energies at the two ends of the film.

While our model is overly simplified, given a lack of knowledge of the details of the interface trap states, it can still give a qualitative picture of the band profile as a function of the value of the Fermi level at the interface.

---

- [1] K. Volz, A. Beyer, W. Witte, J. Ohlmann, I. Nemeth, B. Kunert, and W. Stolz, *J. Crystal Growth* **315**, 37 (2011).
- [2] A. Beyer, I. Nemeth, S. Liebich, J. Ohlmann, W. Stolz, and K. Volz, *J. Appl. Phys.* **109**, 083529 (2011).
- [3] A. Beyer, J. Ohlmann, S. Liebich, H. Heim, G. Witte, W. Stolz, and K. Volz, *J. Appl. Phys.* **111**, 083534 (2012).
- [4] P. Dean, C. Frosch, and C. Henry, *J. Appl. Phys.* **39**, 5631 (1968).
- [5] K. Ishioka, K. Brixius, U. Höfer, A. Rustagi, E. Thatcher, C. Stanton, and H. Petek, *Phys. Rev. B* **92**, 205203 (2015).
- [6] D. Aspnes and A. Studna, *Phys. Rev. B* **27**, 985 (1983).
- [7] T. Dekorsy, T. Pfeifer, W. Kütt, and H. Kurz, *Phys. Rev. B* **47**, 3842 (1993).
- [8] A. V. Kuznetsov and C. J. Stanton, *Phys. Rev. B* **51**, 7555 (1995).
- [9] M. Hase, M. Kitajima, A. Constantinescu, and H. Petek, *Nature* **426**, 51 (2003).
- [10] L. Dhar, J. Rogers, and K. A. Nelson, *Chem. Rev.* **94**, 157 (1994).
- [11] P. Chiaradia, M. Fanfoni, P. Nataletti, P. D. Padova, L. Brillson, M. Slade, R. Viturro, D. Kilday, and G. Margaritondo, *Phys. Rev. B* **39**, 5128 (1989).
- [12] I. Sakata and H. Kawanami, *Appl. Phys. Exp.* **1**, 091201 (2008).
- [13] O. Supplie, M. May, G. Steinbach, O. Romanyuk, F. Grosse, A. Nägelein, P. Kleinschmidt, S. Brückner, and T. Hannappel, *J. Phys. Chem. Lett.* **6**, 464 (2015).
- [14] C. V. de Walle and J. Neugebauer, *Nature* **423**, 626 (2003).
- [15] The assumption of uniform charge distribution is not perfectly consistent with our other assumptions that the surface and interface states fix the Fermi level, which would lead to localized charge densities at the surface and interface. Ignoring these charge densities affects the boundary conditions of the fields across the interface.